Cell PRESS
Structure
Article

Force Generation in Kinesin Hinges on Cover-Neck Bundle Formation

Wonmuk Hwang,[1,*] Matthew J. Lang,[2] and Martin Karplus[3,4,*]
[1]Department of Biomedical Engineering, Texas A&M University, College Station, TX 77843, USA
[2]Department of Biological Engineering & Department of Mechanical Engineering, Massachusetts Institute of Technology, Cambridge, MA 02139, USA
[3]Department of Chemistry and Chemical Biology, Harvard University, Cambridge, MA 02138, USA
[4]Laboratoire de Chimie Biophysique, ISIS Université Louis Pasteur, 67000 Strasbourg, France
*Correspondence: marci@tammy.harvard.edu (M.K.), hwm@tamu.edu (W.H.)
DOI 10.1016/j.str.2007.11.008

SUMMARY

In kinesin motors, a fundamental question concerns the mechanism by which ATP binding generates the force required for walking. Analysis of available structures combined with molecular dynamics simulations demonstrates that the conformational change of the neck linker involves the nine-residue-long N-terminal region, the cover strand, as an element that is essential for force generation. Upon ATP binding, it forms a β sheet with the neck linker, the cover-neck bundle, which induces the forward motion of the neck linker, followed by a latch-type binding to the motor head. The estimated stall force and anisotropic response to external loads calculated from the model agree with force-clamp measurements. The proposed mechanism for force generation by the cover-neck bundle formation appears to apply to several kinesin families. It also elucidates the design principle of kinesin as the smallest known processive motor.

INTRODUCTION

Kinesins, the smallest processive motor proteins known to date, carry out various tasks including cargo transport and mitosis (Asbury, 2005). A conventional kinesin is composed of a ~340 amino acid (AA) N-terminal motor head (MH) possessing ATPase and microtubule (MT) binding activities, a ~485 AA α-helical stalk, and finally a ~92 AA C-terminal domain for cargo binding (Yang et al., 1989). Kinesin typically acts as a dimer where the α-helical stalks form a coiled-coil (Vale, 2003).

Together with G proteins, the kinesin and myosin families share a common "γ-phosphate sensor," including switch I and II (Vale and Milligan, 2000). However, the mechanochemical amplifier coupling the ATPase cycle to force generation appears to have evolved to meet diverse motor needs of the cell, e.g., directionality, processivity, and stall force. Conventional kinesin walks to the plus end of MT and is believed to walk by an asymmetric hand-over-hand mode, although the mechanism is not well understood (Hua et al., 2002; Asbury et al., 2003; Yildiz et al., 2004; Kaseda et al., 2003). The ~12 residue neck linker (NL) connecting MH and the α-helical stalk (Figure 1A) have been shown to play a crucial role in motility (Rice et al., 1999; Wade and Kozielski, 2000). Highly conserved, NL undergoes a large conformational change from a disordered state to a state in which it binds to MH in presence of ATP. Mutations in NL result in impaired motility while the ATPase and MT binding activities of MH are relatively intact (Case et al., 2000; Rice et al., 2003). These results led to the proposal that kinesin generates a walking stroke mediated by NL (Vale and Milligan, 2000), analogous to the power stroke in myosin. Comparison of known kinesin structures largely supports this model since NL is bound to MH only in ATP states (Rice et al., 1999; Skiniotis et al., 2003) (for a comparison between 43 available kinesin structures see Table S2 in the Supplemental Data available with this article online).

The specific mechanism by which ATP binding, hydrolysis, and product release are converted into mechanical force is not known (Block, 2007). The zipper-like docking of NL onto MH after ATP binding has been suggested as the force generating step (Rice et al., 1999; Kikkawa et al., 2001; Sindelar et al., 2002). However, unlike the structurally well-defined lever arm of myosin, NL is much shorter, and is flexible when detached from MH. It is not clear how such a small flexible domain can be involved in force generation. Further, differences in the available structures with bound and unbound NL are small; it is estimated that the MT-bound MH moves only about 3 Å and rotates by only 10°–20° (Kikkawa et al., 2001; Sablin and Fletterick, 2004), in contrast to the change (unkinking) of the relay helix in myosin that is thought to lead to a walking step through a 60°–70° rotation of the converter and lever arm (Geeves and Holmes, 2005). It has also been suggested that NL docking could be initiated by diffusion of the detached trailing head past the bound leading head. In this case, kinesin motility would mainly be Brownian ratchet in nature, with fast equilibrium fluctuations biased by chemical events such as ATP binding (Astumian and Derényi, 1999; Oster and Wang, 2003; Mather and Fox, 2006). However, the basic assumptions of the proposed Brownian ratchet models have not been verified. Thus, it is uncertain whether kinesin uses solely a Brownian ratchet mechanism, a power stroke resulting from a downhill free energy gradient in the forward direction, or a mixture of the two (Block, 2007).

Here, we combine a series of molecular dynamics (MD) simulations and structural analyses to suggest a specific mechanism for the force generation which involves NL. We find that the first half of NL interacts only weakly with the binding pocket on the MH. Consequently, "zippering" per se is insufficient to induce the observed force and has to be assisted by other parts of the

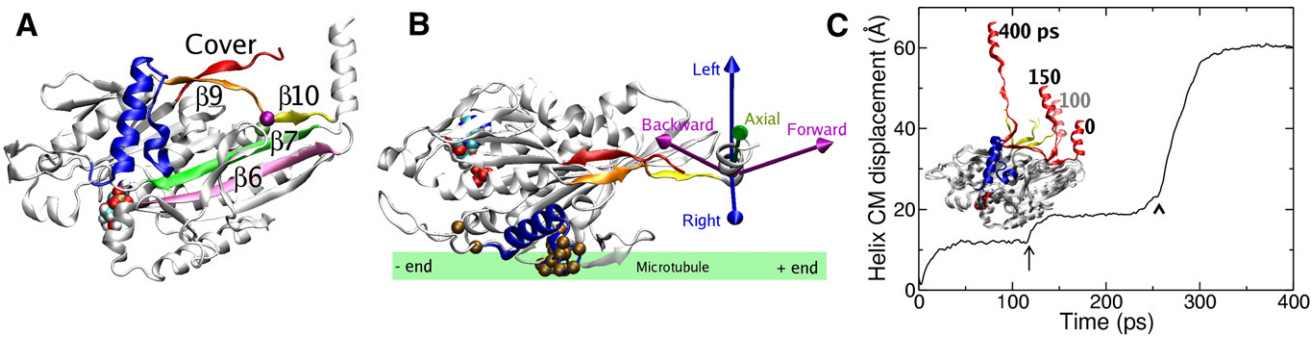

Figure 1. Interaction between NL and MH

(A) X-ray structure of 2KIN. NL consists of β9 (orange) and β10 (yellow), which respectively form β sheets with the N-terminal CS (β0, red) and β7 on the MH core (green). N334 (purple sphere) interacts mainly with G77 (green sphere) and forms the first major bond between NL and MH (Figure S8). The switch II cluster that binds to MT and mediates nucleotide-induced conformational changes through the relay helix α4 (Sablin and Fletterick, 2004, 2001) is in blue as a marker for other figures that display kinesin in different orientations. Molecular drawings are produced by using VMD (Humphrey et al., 1996).

(B) The neck-pulling simulation (Supplemental Data, Text S.2). Brown spheres, anchored atoms in MT binding domains. Five pulling directions were tested based on their orientation relative to MT. In this view, the molecule is rotated approximately 90° about the horizontal axis in (A).

(C) Displacement trajectory of the center of mass of the neck helix pulled with 440 pN in the axial direction (Movie S1). Inset, overlaid snapshots. Viewing direction as in (A). At ~120 ps, one helical turn at the bottom of the pulled helix unwound (arrow), but the N334 latch was held in place until complete unbinding started to occur at ~260 ps (arrowhead), cf., Figure S9.

motor. A structural element, the 9 AA long N-terminal cover strand (CS) (Figure 1), which has not been considered previously, is shown to be crucial for force generation. CS is disordered in the ADP structures with an unbound NL, and forms a β sheet with the first half of NL upon ATP binding. Simulations demonstrate that the resulting cover-neck bundle (CNB) creates a conformational bias that forces NL into the binding pocket of MH by a hinge-like action. After the forward motion, the C-terminal half of NL consolidates binding to MH via a latch mechanism. Kinesin thus possesses a hinge element, but rather than switching between well-defined conformations, as do most myosins, it works by forming and breaking CNB during the mechanochemical cycle.

RESULTS

We used monomeric kinesin structures in PDB: 1BG2, 1MKJ (Sindelar et al., 2002), and 2KIN (Sack et al., 1997). 1BG2 is in the ADP state with an unbound NL. 1MKJ and 2KIN have docked NL and are suggested to be in ATP-like (ADP+SO4) states (use Table S2 as a quick reference for the neck or nucleotide states and Figure S7 for domain names and AA numbers used below). We chose these structures because 1MKJ and 2KIN, together with a dimer structure 3KIN, are the only ones that have the full length of NL, extending to the neck helix, clearly visible in its docked state. Similar to 2KIN, the two heads in 3KIN are in the neck-bound state, which is thought to be incompatible with binding of both heads to MT (Kozielski et al., 1997). Since 3KIN has the lowest resolution (3.1 Å), it was not used. Structural features regarding nucleotide-dependent NL states are also present in other kinesin structures obtained with different nucleotide analogs and cryo-EM structures of the kinesin-MT complex (see Discussion). Thus, our main conclusion for the force generation mechanism is not limited by the structures used for the analysis.

Four sets of analyses were used to develop and support the proposed mechanism. The initial contact analysis of the NL binding pocket revealed that only the C-terminal half of NL has specific interaction with MH, suggesting that NL docking is not affinity driven. This was confirmed by simulations where NL was pulled out of the binding pocket. Next, the unbound NL was found to be flexible with little tendency to dock, while a clear bias is present when it forms a CNB. Thus, a walking stroke is generated by the inherent conformational bias of CNB rather than the binding affinity between NL and MH. Finally, detailed force maps of CNB's walking stroke were constructed to compare with force clamp experiments.

Analysis of the Neck Binding Pocket

NL consists of two β strands, β9 that extends from MH, and β10, which connects to the coiled-coil stalk (Figure 1A). Surprisingly, we found that β9 interacts minimally with MH, except for I327 at the beginning (we use the AA numbering for 2KIN) (Figure S8). A few other contacts between β9 and MH, mainly with L13, are weak and not the same in 1MKJ and 2KIN. Instead, β9 mainly forms a β sheet with CS, while in 1BG2 (unbound NL), NL and CS are separated and disordered. The first major interaction between NL and MH is by N334 located between β9 and β10. It forms two hydrogen bonds, one with G77 (major) and the other with S225. β10 forms a short stretch of β sheet with β7 on MH.

The above observation suggests that NL binding cannot be initiated by an affinity-driven zippering action; β9 (~60% of the length of NL) do not have any strong binding partner. Relatively weak interaction, such as with L13, is unlikely to bring the rearward pointing NL to the forward direction. Binding partners for the rest of NL (G77 and β7) have nearly identical conformations in both ADP and ATP states, as shown by comparing 1BG2 and 1MKJ, and thus cannot directly control the nucleotide-dependent walking stroke generation.

NL Docking Is Locked by the ASN Latch

The interaction between NL and MH was further studied via MD simulations in which NL was forced to unbind (simulation details

are in the Supplemental Data, Text S.2). Certain C_α atoms in the MT binding domains were constrained as anchors to mimic the MT-bound state (brown spheres in Figure 1B). Pulling forces of magnitude 440, 460, and 480 pN were applied to the neck helix in five different directions (Figure 1B). Such large forces were needed to obtain unbinding events during the 0.4–0.8 ns simulation time; this corresponds to previous protein unfolding simulations (Paci and Karplus, 2000; Park et al., 2003). While forced unbinding of NL does not represent the actual unbinding event in kinesin motility, residues important for the NL binding can be highlighted through analysis of the trajectory.

Unbinding proceeded by a rapid initial release of β10, leading to an intermediate state in which N334 was held in place, followed by the release of β9 (Figure 1C and Movie S1). This result is in accord with the above contact analysis: highly conserved (Wade and Kozielski, 2000), N334 acts as a latch that holds NL firmly in the bound state. Once this latch is broken, the β9 part of NL unbinds rapidly (Figure S9) since it does not interact strongly with MH. After full unbinding, no further unfolding occurred until the end of the simulation, suggesting that the MH core is stably folded. In general, a stronger pulling force resulted in faster unbinding (Figure S9). However, at a given force level, the stochastic nature of the process made it difficult to find a clear correlation between the unbinding time and the pulling direction. This would require multiple trajectories, which were not performed since the issue of directional anisotropy is addressed below through the molecular force map.

Orientation of Freely Moving MH

We next constrained the neck helix (a part of the neck coiled-coil stalk) and monitored the motion of the freely moving MH to determine the role of NL in controlling the head motion (Supplemental Data, Text S.3). The following preparations were used: (1) 1MKJ and 2KIN from neck-pulling simulations that preserve the CNB structure; (2) as in (1), but CS removed to determine its role in controlling the head motion; and (3) 1BG2 (originally in the unbound conformation) by attaching the missing NL and the neck helix (AA 326–349), which does not have CNB. In case (1), the unbound MH moves with the CNB formed, while in cases (2 and 3), the MH and the neck helix are connected solely by NL. A spherical coordinate system was used to analyze the head motion (Figure 2A). The position and direction (θ,φ) of the center of mass of MH was followed as a function of time. To quantify the orientation of MH, we chose β6 that spans the MH core (Figure 1A), with the corresponding spherical coordinate (θ_h, ϕ_h); see Figure 2A. Values of θ or θ_h near 90° correspond to MH positioned or oriented, respectively, perpendicular to the neck helix, and $|\phi| < 90°$ ($|\phi_h| < 90°$) indicates that MH is on the leading side of MT (oriented to the plus end of MT).

Figures 2B and 2C and Figure S10 (Movies S2–S4) reveal that the position and orientation of MH fluctuate more when CNB is not formed than when CNB is present (case [1]). In the latter case, NL returned to the binding pocket, nearly restoring the original X-ray structures (Figures S11B and S11D). These simulations are analogous to the situation when an unbound MH is performing a "diffusive search" for the next binding site, with the neck helix (coiled-coil stalk) being less mobile. However, CNB is observed only in the NL-docked ATP structures, corresponding to a MT-bound state (Rice et al., 1999). Case (1) should thus be interpreted conversely, as NL binding to the leading head on MT.

CNB Has a Conformational Bias to Move into the Binding Pocket

The above results indicate that CNB may be responsible for generating the force for a walking stroke. We further tested this by MD simulations with the same atoms anchored as in the neck-pulling simulation (Supplemental Data, Text S.3). For 1MKJ and 2KIN, we performed simulations with unbound structures obtained from neck-pulling simulations, and rebinding-like events of NL were indeed observed (Figures 2D and 2E and Movies S5 and S6). In both cases, CNB bent toward the binding pocket, but the ASN latch and β10 did not form specific bonds with MH within the simulation time. Bending of β9 is due to the conformational bias of CNB, so is captured nearly deterministically in MD simulation, but latching is more specific, which in general cannot be observed within finite simulation times.

In simulations where the unbound MH moved, rebinding of CNB occurred despite deformations of other parts of the molecule at the high simulation temperature (360 K) (Figures S11B and S11D), suggesting that once formed, the biased motion of CNB toward the binding pocket is mostly autonomous. To further test this conclusion, we attached CNB from the simulation of 1MKJ to an originally unbound structure that lacks CNB, 1BG2, and monitored its motion with the atoms at the MT binding interface anchored as above (Supplemental Data, Text S.3). Since 1BG2 is in an ADP-state, bending of the attached CNB would mean that it requires no specific interaction with MH. We indeed observed that CNB bent into the binding pocket (Figures 2F and 2G and Movie S7), although it was displaced sideways by L13 (AA 292–294) that protrudes from the binding pocket (cf., Figure S12). A possible steric role of L13 in NL binding is discussed in the Supplemental Data, Text S.3.

The autonomous bias of CNB was further confirmed by explicit-water simulations of isolated CNBs without the MH core and the base of CNB fixed in space (Supplemental Data, Text S.4). Remarkably, it bent in the direction of the binding pocket even in the absence of MH (Figure S13 and Movie S8), suggesting that the relaxed conformation of an isolated CNB is close to its bound conformation on MH. The main difference from continuum solvent simulations was in time scale; the viscosity effect slowed the bending time from <50 ps in continuum solvent (Figures 2D–2G) to >0.5 ns in explicit water, closer to the actual time scale (Gsponer et al., 2003). From these results, it appears that CNB formation, rather than the global conformational change of MH (e.g., rotation of switch II), initiates the walking motion. Conformational change of MH mainly facilitates CNB formation, after which the forward motion is generated almost entirely by CNB alone. This conclusion is consistent with earlier experiments wherein swapping of the neck domains between conventional kinesin and the minus-end-directed motor NCD reversed the directionality (Wade and Kozielski, 2000; Case et al., 1997; Henningsen and Schliwa, 1997; Endow and Waligora, 1998); attaching CS and the regions after α6 (β9 to the neck helix) respectively to the N and C termini of NCD's catalytic core (i.e., replacing kinesin's MH core with that of NCD) resulted in plus-end-directed-motility (Case et al., 1997). While it is unknown if CNB can still form in the chimera, these experiments support

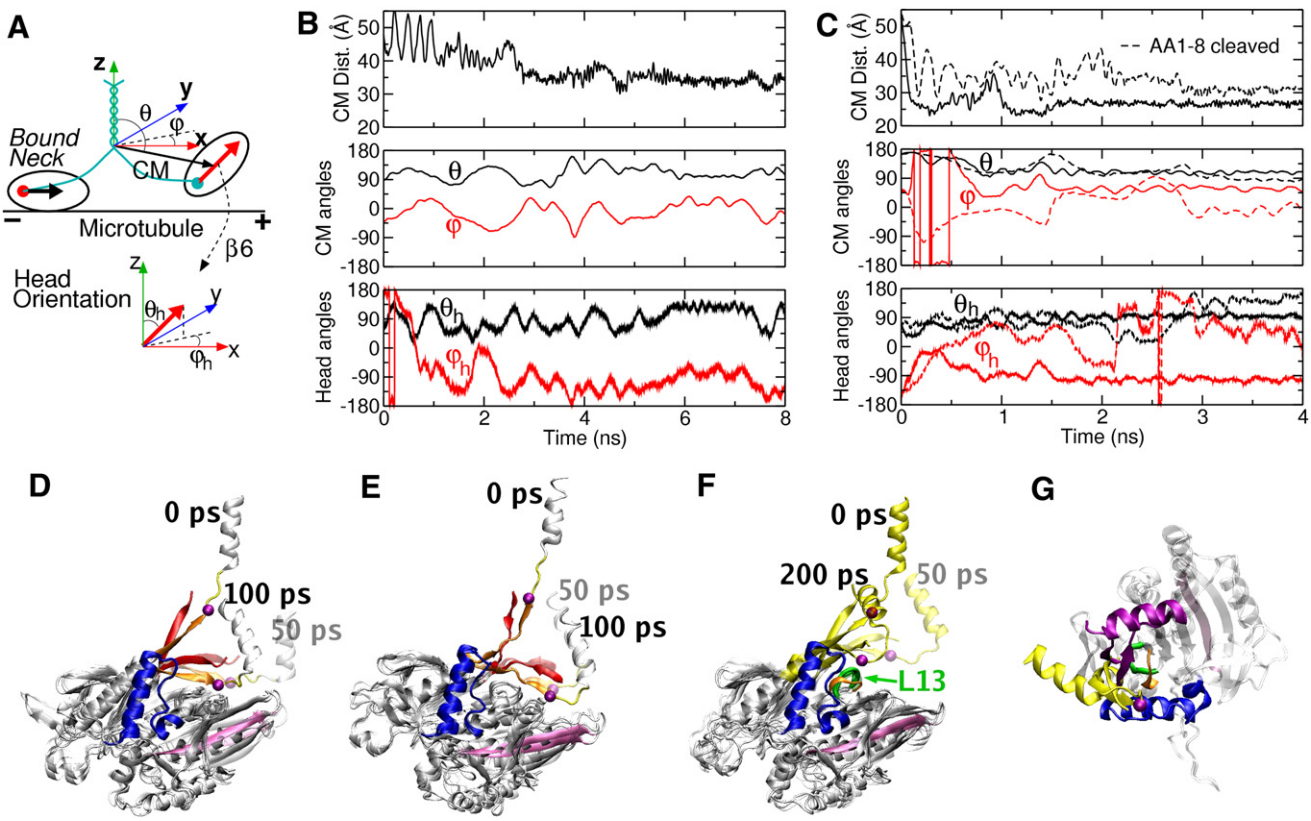

Figure 2. Conformational Bias of CNB

(A–C) Motion of the unbound MH: (A) Coordinate system used for measurement. The z axis, along the neck helix in the MT bound state; the x axis, parallel to β6 when NL is bound to MH (thick black arrow on the trailing head), pointing approximately to the plus end; the y axis is fixed by the right-hand rule. Similar to the center of mass (CM) of MH (θ, ϕ), the MH orientation (θ_h, φ_h) was quantified by using β6 (thick red arrow) as a directional marker. (B) 1BG2, with NL and the neck helix attached (Movie S2). (C) 2KIN. Solid, with CNB (Movie S3), showing a stable trajectory after an initial transient. Dashed, without CS, showing more fluctuations (Movie S4). Azimuthal angles ϕ and ϕh range within $\pm\pi$, causing discrete jumps. Fluctuations attenuate at later times even without CS because the flexible NL binds to MH nonspecifically (Figure S11).

(D–G) Rebinding of CNB (Movies S5–S7). (D) 1MKJ, (E) 2KIN, (F and G) A chimeric 1BG2 with CNB attached. The snapshot at 50 ps is rendered transparent for clarity. (D and F) The neck helix and β10 bounce after 50 ps, but the β9 part stays on MH. (G) Conformation in (F) at 200 ps viewed from the plus end of MT in Figure 1B. Color schemes and viewing directions in (D)–(F) are the same as in Figure 1A. (F and G) The attached CNB and the neck helix are in yellow. (G) Purple, the original bound conformation of CNB/neck helix in 1MKJ (superposed). L13 in 1BG2/1MKJ are in green/orange (cf., Figure S12). In 1BG2, it protrudes from the binding pocket, displacing NL downward (Supplemental Data, Text S.3).

the autonomous action of the neck region without specific binding interactions with MH. Furthermore, analysis of the available structures indicate that MH share the same conformational states, including minus-end-directed kinesins that do not have NL (Wade and Kozielski, 2000; Grant et al., 2007), which suggests that the conformational change of MH is unlikely to be used directly for forward force generation.

The Force Map of CNB Is Consistent with Kinesin's Forward-Biased and Transversely Anisotropic Force Response

An important question regarding the conformational bias of CNB is whether the force exerted by it alone is in accord with the force response of kinesin in experiments (Block et al., 2003). To address this, we devised a way to measure the force exerted by CNB in a given conformational state as a free-energy gradient (Figure 3 and Supplemental Data, Text S.5). The method consists of applying a harmonic sampling potential that retains V331 C_α around a point at which the force is to be measured. The harmonic potential prevents relaxation of CNB and its bent conformation is maintained during the simulation, as illustrated in Figure 3. By analyzing the positional fluctuation of V331 C_α, the force exerted at the center of the sampling potential can be calculated (Supplemental Data, Text S.5). The simulation was performed with an isolated CNB constructed from 1MKJ. For comparison, we also measured forces generated by NL alone. Similar to the explicit water simulation (Figure S13), we kept only up to a portion of NL, β9 to V331, which is the reason why force was measured at V331 C_α. We omitted the N332 latch and β10 since they do not play a major role in force generation.

A total of 2.9 μs MD simulations were performed to obtain force maps over sampling points spaced 2 Å apart (Figure S14), at 300, 330, and 360 K, and at 300 K with NL alone as a control (Supplemental Data, Text S.6). Different temperatures were used to determine if the force is enthalpic or entropic in origin. The direction and magnitude of the force varied from point to point.

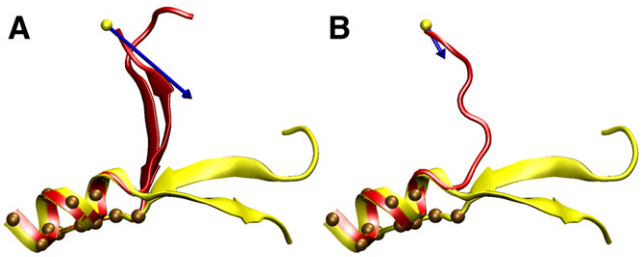

Figure 3. Measurement of the Generated Force

(A and B) By CNB (A) and by NL alone (B). Red, portion of 1MKJ used for the simulation. Brown spheres, C_α atoms constrained as anchors. Yellow ribbon, CNB in its bound conformation, as a guide for the eye. Blue arrow, force applied by V331 C_α at the location marked by the yellow dot (Supplemental Data, Text S.5). The length of the arrow is proportional to the magnitude of the force, where CNB generates a larger force than NL alone does. Calculating forces at different locations of V331 C_α yields the force map in Figure 5 (Supplemental Data, Text S.6).

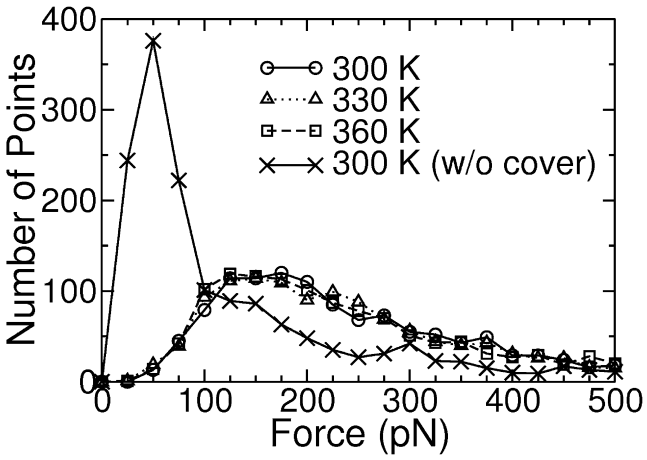

Figure 4. Force Distribution by CNB and NL

Vertical axis, the number of sampling points at which the generated forces fall in the corresponding range (bin size = 25 pN). NL alone generates forces that are peaked at a lower value (~50 pN), although there is a tail of higher forces. As discussed in the text, only the physically more relevant low force regions are displayed in Figure 5.

We first made a histogram of the measured forces (Figure 4). At 300 K, for the CNB, they range within 28.2–4661 pN (peak at ~150 pN). In regions of very large forces, NL is overstretched or bent, corresponding to physically forbidden states. The distribution was very similar at 330 and 360 K, indicative of the enthalpic, rather than entropic origin of the force. In contrast, NL alone, the overall force (1.5–1472 pN) was much lower and narrowly distributed below 100 pN (peak at ~50 pN). Clearly, CNB can exert greater forces than NL alone can.

For the spatial distribution, only low force regions (lower than the peaks in Figure 4) were considered as they are physically most relevant. The resultant force map is a hemispherical shell (Figures 5A and 5B), suggesting that the cutoff of 150 pN was adequate for covering the possible range of CNB's hinged swiveling motion. The force map confirms the overall conformational bias of CNB to move into the binding pocket: we quantified the forward bias of CNB by decomposing the force vectors below 150 pN into longitudinal and transverse components relative to the axis of α6, which is approximately parallel to MT. On average, the longitudinal/transverse components were 46/88 pN, implying a steeper transverse free-energy gradient. Thus CNB tends to be oriented toward in a cone-like energy landscape. Consistent with this, transverse loads in force-clamp experiments have less effect on kinesin motility (Block et al., 2003). On the other hand, forces below 50 pN generated by NL alone had average forward/transverse components of 1.6 pN/24 pN. There were many points with negative forward components, resulting in a small average, confirming the absence of a forward bias by NL alone.

In Figures 5C and 5D, it can be seen that the force vectors point toward the direction of the binding pocket, which was quantitatively verified by a detailed analysis of the angular distribution of force vectors (Figure S15; Supplemental Data, Text S.7). Furthermore, the force map is transversely anisotropic, such that the low force region is populated more on the left side of the direction of the kinesin movement (green arrows in Figures 5A and 5C). This agrees with the two-dimensional force-clamp experiment in which a leftward force causes a greater decrease in the walking velocity than a rightward force (Block et al., 2003). In contrast, NL alone generates less force and has only a small conformational bias or anisotropy, if any. A slice of the force map with and without CS is compared in Figures 5D and 5E. For NL alone, the forces symmetrically point to the axis of α6 rather than to the binding pocket (see also Figure S15), and the low force region is a filled disc rather than a ring, indicating absence of rigid swiveling motion. Thus, NL is flexible without CS so that it cannot generate the force required for the observed bias.

In contrast to the forward bias and directional anisotropy, it is trickier to quantitatively compare the stall force between experiments and our simulations, mainly due to the difference in locations at which forces are measured: in an optical trap, force is applied/measured via a microbead attached along the ~80 nm long neck stalk, while in our simulation, forces act at the end of β9, about 2.3 nm from the base (hinge) of NL. Thus, torques rather than forces must be compared. A detailed analysis suggests that the torque generated by CNB either meets or exceeds that from the force-clamp experiment (Supplemental Data, Text S.8 and Figure S16). Thus, CNB generates enough force to propel kinesin motility.

Last, we performed explicit water simulations at eight sampling points to check whether our results are affected by the choice of force field or solvation model (Supplemental Data, Text S.9). The measured forces were overall comparable to those from implicit solvent simulations (Figure S17), and there is no fundamental change in the conformational bias of CNB. Therefore, the force generated by CNB is robust and provides the structural basis for the response of kinesin in force-clamp experiments.

DISCUSSION

The essential conclusion of the present analysis is that CNB, a β sheet made up of CS and the first half of NL, is the force-generating element in kinesin motility. The two-strand division of NL (β9 and β10) (Figure 1A) is functional: β9, interacting weakly with MH, generates the force required for forward motion through CNB formation, while β10 and the ASN latch ensure stronger,

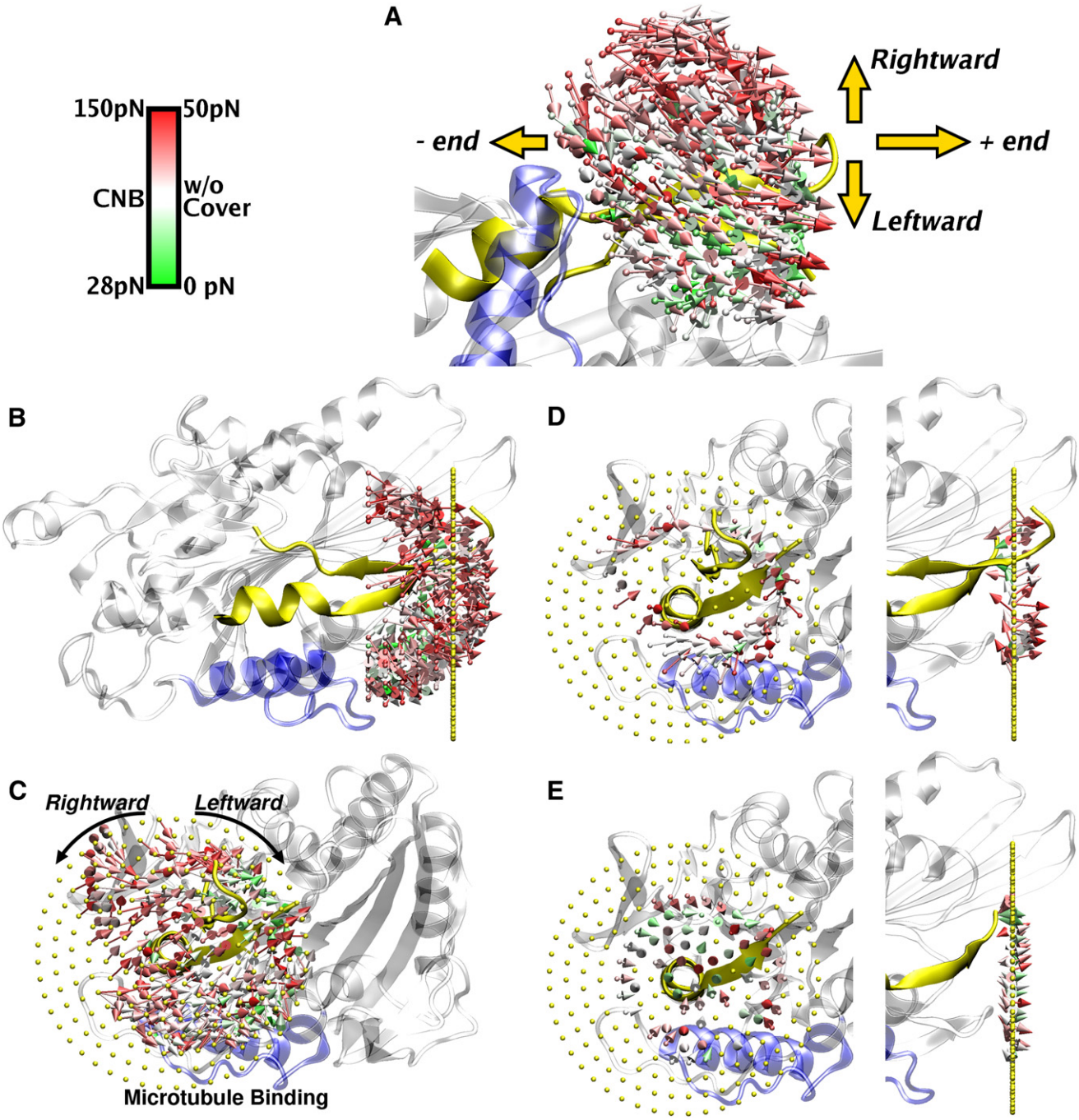

Figure 5. Calculated Force Map

(A–E) For CNB (A–D) and for NL alone (E). Displayed force vectors range from the lowest to those at the peak in Figure 4. Color bars have the corresponding scales and the arrow length is proportional to the force. The dot at the tail of an arrow is the sampling point where V331 C_α exerts the corresponding force. Yellow dot, sampling point where the force is above the maximum in the color bar (not displayed). 1MKJ is superposed as a reference (blue, switch II; yellow ribbon, CNB in the bound conformation, as in Figure 3). (A) A view from the MT binding side. (cf., Figure 1A). Big arrows indicate approximate directions with respect to the plus end of MT. (B) A view in a similar direction as in Figure 1B, revealing the spherical shell structure and the forward bias. The plane defined by yellow dots is used for (D) and (E). (C) A view from the plus end of MT into the axis of α6. In (A) and (C), forces are lower (green) on the leftward side with respect to the direction of motion. (D and E) A slice through the plane in (B). Since the force map is an asymmetric spherical shell, the low force region in (D) is a distorted ring. In (E), it is a filled disc, suggesting that NL alone does not rigidly swivel.

more specific binding, which stabilizes the docked state of NL. From its temperature independence, the conformational bias of CNB appears to be primarily enthalpic, suggesting that its hinge-like action is a power stroke. The anisotropic distribution and magnitude of forces generated by CNB are consistent with force-clamp measurements of the stall force and transverse anisotropy. The proposed mechanism differs from the affinity-driven, zipper-like binding of NL alone, which our calculations show does not possess a bias nor generates a large enough force. Our conclusion is consistent with experiments other than those considered above (Supplemental Data, Text S.10) and also is thermodynamically plausible (Rice et al., 2003) (Supplemental Data, Text S.11).

Two structural features of CNB explain its conformational bias. First, the helical turn at the end of α6 leading to NL, points into the neck binding pocket (Figure 6A, red). Second, CS is located on the left side of NL with respect to the plus-end direction, so that the inherent right-handed chirality of β sheets (Shamovsky et al., 2000) places CS on top of NL, pushing it down and "covering" it (Figure 1A).

Power Stroke Generation by ATP Binding

By comparing 1BG2 (ADP state) and 1MKJ (ATP-like state), we propose how the power stroke is generated upon ATP binding: in the leading head with NL in an undocked, nucleotide free state, switch II (blue in Figure 6A) is close to α6, preventing the formation of its extra helical turn (red) (Sindelar et al., 2002). The unwound portion of α6, which connects directly to β9 of NL, renders it out of register with CS, blocking CNB formation. When ATP binds (**1** in Figure 6A), switch II retracts (**2**), allowing the extra helical turn of α6 to form (**3**). CS and β9 are now in register and form CNB, leading to the power stroke (**4**). Once the forward movement is made, the ASN latch and β10 (Figure 1A and Figure S8) ensure tight binding of NL to MH.

Stepping Mechanism of Kinesin

The force generated by CNB suggests a possible sequence of events for the walking step of kinesin (Figure 6C). When the trailing head detaches from MT upon Pi release (Rosenfeld et al., 2003), CS on both heads are separated from the unbound and flexible NL. The reduced strain on NL of the leading head allows ATP binding (Rosenfeld et al., 2003), leading to CNB formation (Figure 6A) and a power stroke (Figure 6C, middle). Alternatively, the detachment of the trailing head in the ADP state may occur as a result of the power stroke, rather than preceding it. This is a possibility since the weakly bound MH in the ADP state undergoes a rocking motion (Sosa et al., 2001), which might relieve the rearward strain on NL of the leading head (cf., Figure 6B, red dotted), allowing ATP binding. In either case, after the power stroke, the new leading head would perform a diffusive search for the next MT binding site in a narrowly defined region rather than over the entire 16 nm interval. During this time, specific binding of the ASN latch and β10 to MH is established, which would in turn assist in the correct positioning of the leading head. It is also possible that binding to MT by the new leading head may promote latching of NL in the trailing head after power stroke. The mechanism that involves a power stroke followed by a diffusive search is consistent with two substeps observed in experiments, a fast ~25 μs step followed by a slower one (Nishiyama et al., 2001; Rosenfeld et al., 2001). After the initial power stroke, binding of the new leading head to MT could take longer due to its diffusive nature. In the case of myosin V, a 25 nm step involving a power stroke followed by a smaller biased diffusion over 11 nm has also been observed (Veigel et al., 2002), although the details of the steps are likely to differ in the two motors. However, the existence of substeps is still under debate (Block, 2007) and the diffusive search could be fast in a narrow range, rendering no detectable substep (Carter and Cross, 2005). Further clarification of the coordination between MHs in kinesin motility requires simulation of the dimer on MT, as an extension of the present work.

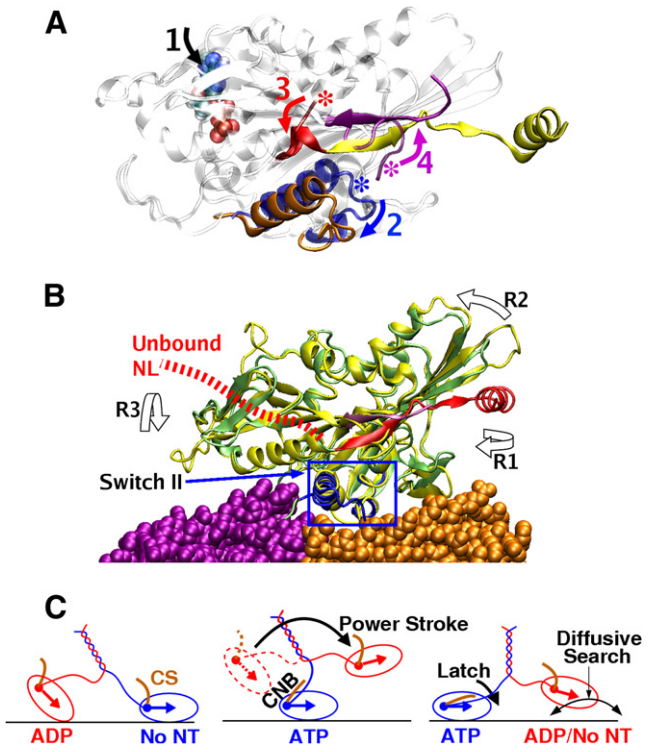

Figure 6. Conformation-Dependent Power Stroke Generation

(A) Possible pathway of CNB formation upon ATP binding. Viewing direction is as in Figure 1B. Relevant domains in 1BG2/1MKJ are: switch II, blue/orange; additional turn of α6 helix, red; CS, purple; and NL/helix, yellow. Marked in stars are the conformations in 1BG2. Both CS (purple star) and NL (red star) are disordered; while CS in 1BG2 is visible, its B factor is high and is invisible in other ADP structures with unbound NL (Figure S12).

(B) Kinesin-MT interface. 2KIN (green and red) is superposed to KIF1A (yellow) in its MT-bound structure (1IA0) (Kikkawa et al., 2000), with an rmsd of 1.5 Å . R1–R3, three rotational modes upon ATP binding, which could reduce the rearward strain on an unbound NL (dotted red).

(C) CNB-assisted stepping mechanism. Left, Pi release in the trailing head causes it either to dissociate or to be only weakly bound to MT. Middle, ATP binding to the leading head results in a power stroke through CNB formation, moving the trailing head forward. Right, the new leading head diffusively searches for its MT binding site, or is weakly bound in a mobile state until ADP release.

Cover Strand in Other Kinesins

If the role of CS in force generation is a general mechanism, similar features should be found in other kinesins. An analysis

Table 1. Comparison between the Cover Strand Sequences

SwissProt ID	Organism					1		3		**5**		**7**		**9**
(2KIN)	Rat	-	-	-	-	M	A	D	P	**A**	E	**C**	S	**I**
(1MKJ)	Human	-	-	-	-	M	A	D	L	**A**	E	**C**	N	**I**
P28738	Mouse	-	-	-	-	M	A	D	P	**A**	E	**C**	S	**I**
Q6V1L4	Quail	-	-	-	-	M	A	D	P	**T**	E	**C**	S	**I**
Q504B9	Zebrafish	-	-	-	M	T	D	A	A	**A**	E	**C**	N	**I**
Q4S807	Puffer	-	-	-	M	A	D	V	P	**A**	E	**C**	N	**I**
Q3MHM9	Bovine	-	-	-	-	M	A	D	P	**A**	E	**C**	N	**I**
P35978	Sea urchin	-	-	-	-	M	A	D	P	**A**	E	**C**	N	**I**
Q5R9K7	Orangutan	-	-	-	M	A	E	T	N	**N**	E	**C**	S	**I**
P21613	Squid	-	-	-	-	M	D	V	A	**S**	E	**C**	N	**I**
P17210	Drosophila	M	S	A	E	R	E	I	P	**A**	E	**D**	S	**I**
(1I6I; KIF1A)	Mouse	-	-	-	-	-	-	-	M	**A**	G	**A**	S	**V**
(1Q0B; EG5)	Human	S	S	A	K	K	K	E	E	**K**	G	**K**	N	**I**

Top right row, residue numbers in 2KIN and 1MKJ. Residues that form backbone hydrogen bonds with NL are in bold. Names in parentheses indicate that the sequences are from the corresponding PDB. In EG5, the first residue is S6.

of 43 available PDB structures of kinesin (Supplemental Data, Text S.12) reveals that CNB is observed in most ATP-like structures in Kinesin families 1, 3, and 5 (cf., Figure S12) (family names are from Lawrence et al. [2004]), although its visibility varies possibly due to the transient nature of CNB. In agreement with structural comparison, sequence analysis suggests that force generation by CNB is likely to apply to at least Kinesin-1, -3, and -5. A BLAST search (http://ca.expasy.org/tools/blast/) using the 2KIN sequence reveals conservation in the sequence of CS, mostly in the Kinesin-1 family (Table 1). CNB formation is initiated by the conserved I9, which is replaced by V6 in 1I6I (KIF1A). Both residues have high β sheet propensities, with ILE the highest, and VAL the third highest (Kim and Berg, 1993). The homology decreases toward the N terminus and the length of CS also varies (for 1Q0B, the first residue in Table 1 is S6). Variations in length and sequence of CS, and the portion of CS that forms a β sheet with β9 of NL, could be a way to fine-tune the duration and strength of the power stroke in kinesins that carry out different tasks. For example, the long CS of EG5 may be related to its ability to withstand high loads (Valentine et al., 2006).

In the minus-end-directed NCD (Kinesin-14), the coiled-coil stalk precedes the motor head (C-terminal motor). Instead of a flexible NL, an α-helical neck continues from the neck stalk, connecting to the motor head (Sablin et al., 1998). As it walks nonprocessively (Case et al., 1997), NCD does not need to have both heads bound to two tubulin subunits, so that a flexible NL is not required to make possible the stretching of the two motor heads between binding sites. Its walking stroke may be mediated by conformational changes that involve lever-arm-type switching between two specific binding interactions (Wendt et al., 2002; Endres et al., 2006). Despite this difference, the ASN latch in NCD has been postulated to control the movement of neck/stalk (Endow, 2003). Similar to CS, NCD also has an ~36 AA C-terminal domain that is not visible in available structures (Endow and Waligora, 1998). Together with the neck, this domain was identified to be separate from the catalytic core that is conserved and structurally similar to that of the conventional kinesin (Sablin et al., 1996; Wade and Kozielski, 2000). Replacing the C-terminal domain with kinesin's NL decreased the motor velocity by 10-fold (Endow and Waligora, 1998). Thus the C-terminal "cover" domain of NCD might play a role similar to that of the cover strand by assisting the motion of the neck. Taken together, the wide distribution of CS or the cover domain suggests they may play general roles in force generation in the kinesin families.

Kinesin-MT Interaction

It should be noted that currently available X-ray structures are obtained from isolated kinesins, which might be different from those bound to MT, where force generation occurs during the kinesin mechanochemical cycle. However, cryo-EM structures of KIF1A-MT complexes in ADP and ATP analogs (AMPPNP and AMPPCP) (Table S2) (Kikkawa et al., 2000; Kikkawa and Hirokawa, 2006) reveal no deviation from isolated X-ray structures that would suggest CNB formation could not happen, where the ATP analog structure also superposes well with 2KIN (Figure 6B). The major difference between the two observed states is the motor core rotation (see below), consistent with the proposed role of CNB in the power stroke and latching of β10 when kinesin interacts with MT. For the Kinesin-14 motor KAR3, a large conformational change of MH catalyzed by interaction with MT was observed (Hirose et al., 2006). However, Kinesin-14 does not possess NL, and even the observed changes are mostly in the nucleotide binding pocket and in the central β sheet, away from the neck region.

Three semiorthogonal rotational modes of MH have been observed upon ATP binding (R1–R3 in Figure 6B). A clockwise ~20° rotation in the plane of the MT surface (R1) (Kikkawa et al., 2001), tilting up (R2) (Kikkawa et al., 2001), and a clockwise 20.6° rotation along the MT axis viewed from the plus end (R3) (Kikkawa and Hirokawa, 2006) (cf., **2** in Figure 6A, with switch II attached to MT). These rotations can decrease the angle between the neck binding pocket and the rearward pointing NL, reducing the rearward strain and promoting CNB formation. Conversely, ATP hydrolysis is expected to produce opposite rotations, which would weaken the binding of β10. At the same time, rotation of switch II opposite to **2** in Figure 6B would break

the extra turn of α6, so that the opening of CNB may start from the N terminus of β9. Similar to α6, unwinding of the SH1 helix has been proposed to control the reverse-directed walk of myosin VI (Ménétrey et al., 2005).

MH cores of kinesins are known to be very similar, with an average root mean square deviation (rmsd) of 1.59 Å (Grant et al., 2007). This includes the proximity between the N and C termini of the core (Wade and Kozielski, 2000), which is a necessary condition for CNB formation. As we demonstrated through extensive simulations, the conformational bias of CNB is a local property that arises from the conformational relaxation of the β sheet itself (cf., Figure S13), thus is unlikely to be affected by slight changes in the MH conformation that might occur when bound to MT. In the unlikely case when the conformational change is more extensive and prevents CNB formation, the forward motion of NL should be driven by thermal motion, since our calculation shows that NL alone possesses little forward bias. Furthermore, even if the binding pocket of β9 on MH (such as L13) were to change conformation in a previously unobserved manner and to interact more strongly with β9 than analyzed here (Figure S8), the altered conformation of the binding pocket still would not be able to initiate the forward motion due to its separation from the rearward pointing NL, as depicted in Figure 6B. Thus, the stepping motion of MH without CNB formation is expected to be Brownian ratchet in nature. However, currently there are no experimental data supporting this scenario. See Supplemental Data, Text S.10, for further discussion about the potential role of the Brownian ratchet mechanism in kinesin motility.

Mechanical Design of Kinesin

Another processive motor, myosin V, has a long lever arm that amplifies small conformational changes at the active site of MH into a large step along F-actin. In comparison, CNB in kinesin may be described as a "transient" lever arm. While MH rotation upon ATP binding is small, the bending of CNB can be larger than 90° (Figure S13D), which is achieved through a dynamical β-sheet formation. This suggests that CNB is a transient force-generating element, which is adapted to a small processive motor such as kinesin: when CNB is not formed, the flexible NL allows both heads to bind to MT, ensuring processivity (Rosenfeld et al., 2003). When formed, CNB can generate a power stroke without requiring a relatively rigid lever arm such as in myosin, which is about four times larger than kinesin. Further, the latch mechanism involving only half of NL instead of its full length is appropriate since developing more binding partners on the small MH would be difficult without disrupting the highly conserved nucleotide sensing machinery (Vale and Milligan, 2000). It also makes NL easier to unbind when required during the mechanochemical cycle.

The dynamic nature of CNB formation could be the reason why a role for CS has not been suggested previously, even though the structures discussed in this paper have been available for some time. Only through extensive simulations was it possible to recognize CNB as a force-generating element. Although the model is largely supported by the available data, additional experiments are needed to test the conclusions in more detail and to determine whether they must be modified to obtain a more accurate description of kinesin function. Because the force generation mechanism, based on a disorder-order transition of the CNB, was recognized by physics-based simulations, it is suggested that other transport motors would benefit from corresponding analyses.

EXPERIMENTAL PROCEDURES

Simulation Methods

For simulation, we used CHARMM (Brooks et al., 1983) version 31b1. The simulation setup, data management, and analysis were performed by using custom C++ codes and the BASH scripting language in the Linux operating system. Further details are given in the Supplemental Data.

Supplemental Data

Supplemental Data include seventeen figures, Supplemental Experimental Procedures containing details of simulation methods, as well as additional data, discussion, movies, and references and are available at http://www.structure.org/cgi/content/full/16/1/62/DC1/.

ACKNOWLEDGMENTS

This work was supported in part by a grant from the National Institute of Health (NIH) for M.K. and NIH 1R21 NS058604-01 for W.H and M.J.L. We thank Jeff Gelles for helpful discussions.

Received: August 22, 2007
Revised: October 31, 2007
Accepted: November 2, 2007
Published: January 8, 2008

REFERENCES

Asbury, C.L. (2005). Kinesin: world's tiniest biped. Curr. Opin. Cell Biol. *17*, 89–97.

Asbury, C.L., Fehr, A.N., and Block, S.M. (2003). Kinesin moves by an asymmetric hand-over-hand mechanism. Science *302*, 2130–2134.

Astumian, R.D., and Derényi, I. (1999). A chemically reversible Brownian motor: application to kinesin and ncd. Biophys. J. *77*, 993–1002.

Block, S.M. (2007). Kinesin motor mechanics: binding, stepping, tracking, gating, and limping. Biophys. J. *92*, 2986–2995.

Block, S.M., Asbury, C.L., Shaevitz, J.W., and Lang, M.J. (2003). Probing the kinesin reaction cycle with a 2D optical force clamp. Proc. Natl. Acad. Sci. USA *100*, 2351–2356.

Brooks, B.R., Bruccoleri, R.E., Olafson, B.D., States, D.J., Swaminathan, S., and Karplus, M. (1983). Charmm: a program for macromolecular energy, minimization, and dynamics calculations. J. Comp. Chem. *4*, 187–217.

Carter, N.J., and Cross, R.A. (2005). Mechanics of the kinesin step. Nature *435*, 308–312.

Case, R.B., Pierce, D.W., Hom-Booher, N., Hart, C.L., and Vale, R.D. (1997). The directional preference of kinesin motors is specified by an element outside of the motor catalytic domain. Cell *90*, 959–966.

Case, R.B., Rice, S., Hart, C.L., Ly, B., and Vale, R.D. (2000). Role of the kinesin neck linker and catalytic core in microtubule-based motility. Curr. Biol. *10*, 157–160.

Endow, S.A. (2003). Kinesin motors as molecular machines. Bioessays *25*, 1212–1219.

Endow, S.A., and Waligora, K.W. (1998). Determinants of kinesin motor polarity. Science *281*, 1200–1202.

Endres, N.F., Yoshioka, C., Milligan, R.A., and Vale, R.D. (2006). A lever-arm rotation drives motility of the minus-end-directed kinesin ncd. Nature *439*, 875–878.

Geeves, M.A., and Holmes, K.C. (2005). The molecular mechanism of muscle contraction. Adv. Prot. Chem. *71*, 161–193.

Grant, B.J., McCammon, J.A., Caves, L.S.D., and Cross, R.A. (2007). Multivariate analysis of conserved sequence-structure relationships in kinesins: coupling of the active site and a tubulin-binding subdomain. J. Mol. Biol. *368*, 1231–1248.

Gsponer, J., Haberthür, U., and Caflisch, A. (2003). The role of side-chain interactions in the early steps of aggregation: molecular dynamics simulations of an amyloid-folding peptide from the yeast prion Sup35. Proc. Natl. Acad. Sci. USA *100*, 5154–5159.

Henningsen, U., and Schliwa, M. (1997). Reversal in the direction of movement of a molecular motor. Nature *389*, 93–95.

Hirose, K., Akimaru, E., Akiba, T., Endow, S.A., and Amos, L.A. (2006). Large conformational changes in a kinesin motor catalyzed by interaction with microtubules. Mol. Cell *23*, 913–923.

Hua, W., Chung, J., and Gelles, J. (2002). Distinguishing inchworm and hand-over-hand processive kinesin movement by neck rotation measurements. Science *295*, 844–848.

Humphrey, W., Dalke, A., and Schulten, K. (1996). VMD: visual molecular dynamics. J. Mol. Graph. *14*, 33–38.

Kaseda, K., Higuchi, H., and Hirose, K. (2003). Alternate fast and slow stepping of a heterodimeric kinesin molecule. Nat. Cell Biol. *5*, 1079–1082.

Kikkawa, M., and Hirokawa, N. (2006). High-resolution cryo-EM maps show the nucleotide binding pocket of KIF1A in open and closed conformations. EMBO J. *25*, 4187–4194.

Kikkawa, M., Okada, Y., and Hirokawa, N. (2000). 15 Å resolution model of the monomeric kinesin motor, KIF1A. Cell *100*, 241–252.

Kikkawa, M., Sablin, E.P., Okada, Y., Yajima, H., Fletterick, R.J., and Hirokawa, N. (2001). Switch-based mechanism of kinesin motors. Nature *411*, 439–445.

Kim, C.A., and Berg, J.M. (1993). Thermodynamic β-sheet propensities measured using a zinc-finger host peptide. Nature *362*, 267–270.

Kozielski, F., Sack, S., Marx, M., Thormählen, M., Schönbrunn, E., Biou, V., Thomson, A., Mandelkow, E.-M., and Mandelkow, E. (1997). The crystal structure of dimeric kinesin and implications for microtubuledependent motility. Cell *91*, 985–994.

Lawrence, C.J., Dawe, R.K., Christie, K.R., Cleveland, D.W., Dawson, S.C., Endow, S.A., Goldstein, L.S.B., Goodson, H.V., Hirokawa, N., Howard, J., et al. (2004). A standardized kinesin nomenclature. J. Cell Biol. *167*, 19–22.

Mather, W.H., and Fox, R.F. (2006). Kinesin's biased stepping mechanism: amplification of neck linker zippering. Biophys. J. *91*, 2416–2426.

Ménétrey, J., Bahloul, A., Wells, A.L., Yengo, C.M., Morris, C.A., Sweeney, H.L., and Houdusse, A. (2005). The structure of the myosin VI motor reveals the mechanism of directionality reversal. Nature *435*, 779–785.

Nishiyama, M., Muto, E., Inoue, Y., Yanagida, T., and Higuchi, H. (2001). Substeps within the 8-nm step of the ATPase cycle of single kinesin molecules. Nat. Cell Biol. *3*, 425–428.

Oster, G., and Wang, H. (2003). How protein motors convert chemical energy into mechanical work. In Molecular Motors, M. Schliwa, ed. (Weinheim, Germany: Wiley-VCH), pp. 207–227.

Paci, E., and Karplus, M. (2000). Unfolding proteins by external forces and temperature: the importance of topology and energetics. Proc. Natl. Acad. Sci. USA *97*, 6521–6526.

Park, S., Khalili-Araghi, F., Tajkhorshid, E., and Schulten, K. (2003). Free energy calculation from steered molecular dynamics simulations using Jarzynski's equality. J. Chem. Phys. *119*, 3559–3566.

Rice, S., Lin, A.W., Safer, D., Hart, C.L., Naberk, N., Carragher, B.O., Cain, S.M., Pechatnikova, E., Wilson-Kubalek, E.M., Whittaker, M., et al. (1999). A structural change in the kinesin motor protein that drives motility. Nature *402*, 778–784.

Rice, S., Cui, Y., Sindelar, C., Naber, N., Matuska, M., Vale, R., and Cooke, R. (2003). Thermodynamic properties of the kinesin neck-region docking to the catalytic core. Biophys. J. *84*, 1844–1854.

Rosenfeld, S.S., Jefferson, G.M., and King, P.H. (2001). ATP reorients the neck linker of kinesin in two sequential steps. J. Biol. Chem. *276*, 40167–40174.

Rosenfeld, S.S., Fordyce, P.M., Jefferson, G.M., King, P.H., and Block, S.M. (2003). Stepping and stretching: how kinesin uses internal strain to walk processively. J. Biol. Chem. *278*, 18550–18556.

Sablin, E.P., and Fletterick, R.J. (2001). Nucleotide switches in molecular motors: structural analysis of kinesins and myosins. Curr. Opin. Struct. Biol. *11*, 716–724.

Sablin, E.P., and Fletterick, R.J. (2004). Coordination between motor domains in processive kinesins. J. Biol. Chem. *279*, 15707–15710.

Sablin, E.P., Kull, F.J., Cooke, R., Vale, R.D., and Fletterick, R.J. (1996). Crystal structure of the motor domain of the kinesin-related motor ncd. Nature *380*, 555–559.

Sablin, E.P., Case, R.B., Dai, S.C., Hart, C.L., Ruby, A., Vale, R.D., and Fletterick, R.J. (1998). Direction determination in the minus-end-directed kinesin motor ncd. Nature *395*, 813–816.

Sack, S., Müller, J., Marx, A., Thormählen, M., Mandelkow, E.-M., Brady, S.T., and Mandelkow, E. (1997). X-ray structure of motor and neck domains from rat brain kinesin. Biochemistry *36*, 16155–16165.

Shamovsky, I.L., Ross, G.M., and Riopelle, R.J. (2000). Theoretical studies on the origin of β-sheet twisting. J. Phys. Chem. B *104*, 11296–11307.

Sindelar, C.V., Budny, M.J., Rice, S., Naber, N., Fletterick, R., and Cooke, R. (2002). Two conformations in the human kinesin power stroke defined by x-ray crystallography and EPR spectroscopy. Nat. Struct. Biol. *9*, 844–848.

Skiniotis, G., Surrey, T., Altmann, S., Gross, H., Song, Y.-H., Mandelkow, E., and Hoenger, A. (2003). Nucleotide-induced conformations in the neck region of dimeric kinesin. EMBO J. *22*, 1518–1528.

Sosa, H., Peterman, E.J., Moerner, W., and Goldstein, L.S. (2001). Adp-induced rocking of the kinesin motor domain revealed by single-molecule fluorescence polarization microscopy. Nat. Struct. Biol. *8*, 540–544.

Vale, R.D. (2003). The molecular motor toolbox for intracellular transport. Cell *112*, 467–480.

Vale, R.D., and Milligan, R.A. (2000). The way things move: looking under the hood of molecular motor proteins. Science *288*, 88–95.

Valentine, M.T., Fordyce, P.M., Krzysiak, T.C., Gilbert, S.P., and Block, S.M. (2006). Individual dimers of the mitotic kinesin motor Eg5 step processively and support substantial loads in vitro. Nat. Cell Biol. *8*, 470–476.

Veigel, C., Wang, F., Bartoo, M.L., Sellers, J.R., and Molloy, J.E. (2002). The gated gait of the processive molecular motor, myosin V. Nat. Cell Biol. *4*, 59–65.

Wade, R.H., and Kozielski, F. (2000). Structural links to kinesin directionality and movement. Nat. Struct. Biol. *7*, 456–460.

Wendt, T.G., Volkmann, N., Skiniotis, G., Goldie, K.N., Müller, J., Mandelkow, E., and Hoenger, A. (2002). Microscopic evidence for a minus-end-directed power stroke in the kinesin motor ncd. EMBO J. *21*, 5969–5978.

Yang, J.T., Laymon, R.A., and Goldstein, L.S.B. (1989). A three-domain structure of kinesin heavy chain revealed by DNA sequence and microtubule binding analyses. Cell *56*, 879–889.

Yildiz, A., Tomishige, M., Vale, R.D., and Selvin, P.R. (2004). Kinesin walks hand-over-hand. Science *303*, 676–678.